Inorganic Chemistry

Article

pubs.acs.org/IC

Platinum Uptake and Ba_2CePtO_6 Formation During in Situ $BaCe_{1-x}M_xO_{3-\delta}$ (M = La, In) Formation

Joey A. Lussier,[†] Shahid P. Shafi,[†] Ronald L. Donaberger,[‡] and Mario Bieringer*[,†]

[†]Department of Chemistry, University of Manitoba, Winnipeg, MB R3T 2N2, Canada

[‡]Canadian Neutron Beam Centre, Chalk River Laboratories, Chalk River, ON K0J 1J0 Canada

ABSTRACT: We report the formation, structures, temperature-dependent phase transitions, and high-temperature reactivity of the potential proton and oxide ion conductors $BaCe_{1-x}M_xO_3$ (M^{3+} = In^{3+}, La^{3+}). The present in situ diffraction studies show oxidative platinum uptake at temperatures as low as 950 °C into $BaCeO_3$, forming the cubic Ba_2CePtO_6 double perovskite. The transient B-site double perovskite expels platinum at around 1200−1250 °C. Platinum oxidation via $BaCeO_3$ is investigated by in situ powder X-ray and neutron diffraction experiments in various atmospheres. Doped $BaCe_{1-x}M_xO_3$ phases show the formation of Ba_2CePtO_6 without incorporating the M^{3+} dopant. Oxidative platinum uptake is also observed during the synthesis of $BaCeO_3$ on platinum metal. We report the reaction pathway for the low-temperature oxidative formation of Ba_2CePtO_6 and the subsequent liberation of platinum for the barium cerate system. The findings are supported by ambient-temperature X-ray diffraction, in situ powder X-ray, and powder neutron diffraction as well as XPS.

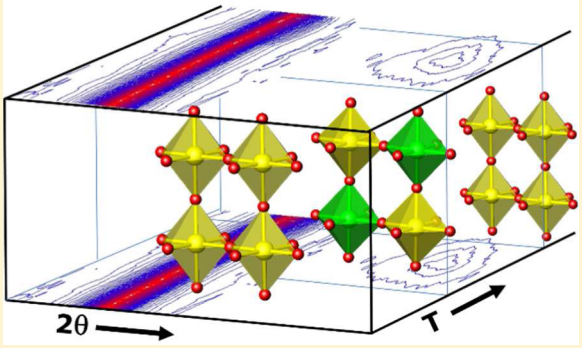

1. INTRODUCTION

The perovskite structure (ABO_3) is the basis for many magnetic, ferroelectric, dielectric, multiferroic, thermoelectric, catalytic, and ion conducting materials and is found in a plethora of devices and applications. The diverse functions of perovskite phases are due to their structural and compositional tolerance and being capable of accommodating almost any cation.[1] During the last 25 years, proton conducting perovskites have been investigated intensely for applications in electrochemical devices, such as fuel cells, sensors, H_2 generation, and extraction.[2−5] One of these perovskites of interest for solid-state proton conduction applications is the cation-doped barium cerate. Doped $BaCeO_3$ compounds are electronic insulators and thus find applications as solid-state proton conductors in fuel cells.[6] The ion conductivity in extended structures is closely related to the presence of defects. Defects in $BaCeO_3$ are created by means of substituting Ce^{4+} with trivalent cations.[7,8] Barium cerates doped with lanthanides were originally studied over 25 years ago by Virkar and Maiti.[9] Notably, trivalent lanthanides are good B-site dopants for $BaCeO_3$ and capable of introducing oxygen defects.

Understanding the detailed structures and phase stabilities at high temperatures is crucial for optimizing the performance of solid oxide fuel cell materials because of their high operating temperature. Knight and Bonanos reported the structural phase transitions in the parent $BaCeO_3$ between 25 and 1000 °C using powder neutron diffraction.[10−12] The room-temperature structure of $BaCeO_3$ is orthorhombic, *Pnma* (space group No. 62), with a phase transition to a second orthorhombic structure, *Imma* (space group No. 74), at 562 K. Above 673 K, $BaCeO_3$ is rhombohedral, $R\bar{3}c$ (space group No. 167), and above 1173 K, the structure is cubic, $Pm\bar{3}m$ (space group No. 221).[13] Figure 1 illustrates the phase transition sequence as reported by Knight for undoped $BaCeO_3$.

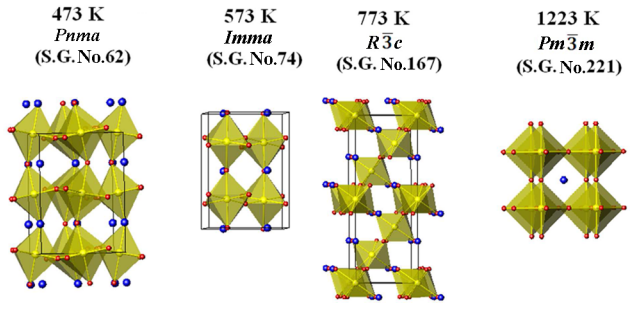

Figure 1. Crystal structures of the four phases of $BaCeO_3$ upon increasing temperature from left to right. Blue spheres = Ba^{2+}, yellow spheres = Ce^{4+}, red spheres = O^{2-}. Yellow octahedra represent CeO_6 octahedra found in all four structures.

During our work on indium-doped barium cerate,[14] we observed an unexplained, transient phase at high temperatures in our in situ X-ray diffraction experiments. The X-ray diffraction peaks at around 2θ = 52.5−53° and at 2θ = 29.6−30° (Cu−Kα radiation) were only observed at temperatures higher than previously measured by Knight and Bonanos (T_{max}

Received: June 24, 2014
Published: August 4, 2014

   dx.doi.org/10.1021/ic501510u | *Inorg. Chem.* 2014, 53, 8809−8815

= 1273 K)[10] and by Scherban and co-workers (T_{max} = 1073 K).[15,16] These peaks indicate either a phase transition or a product decomposition. Interestingly, the peaks only exist over a small temperature range above which the cubic $BaCeO_3$ phase is observed.

This unknown phase has been identified as the double perovskite Ba_2CePtO_6. It was first reported by Ouchetto et al.,[17] when heating $BaCeO_3$ in a Pt crucible in air. Ouchetto et al. did not pursue the Ba_2CePtO_6 phase further.[18] In 2007, Casapu et al. noted Ba_2CePtO_6 while working on a Pt/Ba/CeO_2 catalyst and proposed a reaction in which a $BaPtO_3$ perovskite is first formed, which then reacts with $BaCeO_3$ to form the double perovskite.[19] To our knowledge, these are the only published data on this material, which show surprisingly low reaction temperatures for reaction with platinum.

In the present work, we explore the synthesis and phase diagram of lightly doped $BaCeO_3$ with In^{3+}, La^{3+}, Ho^{3+}, Y^{3+}, Lu^{3+} and compare the results with the parent $BaCeO_3$ system. Using in situ X-ray and neutron diffraction, the formation of Ba_2CePtO_6 is presented. The oxidative platinum(IV) incorporation into $BaCeO_3$ is explored in light of the surprisingly low reaction temperature between platinum metal and $BaCeO_3$. The dopant uptake of $BaCeO_3$ is also studied, and we contrast this with the lack of dopant incorporation into the Ba_2CePtO_6 structure.

2. EXPERIMENTAL SECTION

2.1. Synthesis. *2.1.1. Doped $BaCeO_3$.* Bulk samples ($m \approx 1$ g) of $BaCe_{0.9}M_{0.1}O_{3-\delta}$ and $BaCe_{0.8}A_{0.2}O_{3-\delta}$ (M = La, Ho, Y, Lu, and In; A = In) were prepared from stoichiometric amounts of $BaCO_3$ (Alfa Aesar, 99.95%), CeO_2 (Alfa Aesar, 99.99%), and M_2O_3 (La_2O_3, Ho_2O_3, Y_2O_3, In_2O_3: Cerac, 99.999%, and Lu_2O_3: Alfa Aesar, 99.99%). The starting materials were ground in acetone in an agate mortar and reacted for 24 h in air at 1500 °C in alumina crucibles according to eq 1.

$$BaCO_3 + (1 - x)CeO_2 + (x/2)M_2O_3 \rightarrow BaCe_{1-x}M_xO_{3-\delta} + CO_2 \quad (1)$$

Undoped $BaCeO_3$ was prepared as a reference sample using the same conditions.

2.1.2. Ex Situ Ba_2CePtO_6. Previously prepared $BaCeO_3$ was ground with acetone in an agate mortar with stoichiometric amounts of Pt sponge (Alfa Aesar 99.98%) and reacted in flowing oxygen for 80 h at 950 °C in alumina crucibles according to eq 4. The samples were then quenched to room temperature by removing them from the hot furnace. The samples were then ground and reheated for an additional 264 h under the same conditions.

2.2. Powder X-ray Diffraction. *2.2.1. Room-Temperature Diffraction.* Room-temperature powder X-ray diffraction was carried out using a PANalytical X'Pert Pro diffractometer in Bragg–Brentano geometry equipped with a Cu anode ($\lambda(K\alpha_1)$ = 1.540598 Å, and $\lambda(K\alpha_2)$ = 1.544426 Å), a diffracted beam Ni filter, and an X'Celerator detector. Using acetone slurries, the samples were mounted as thin layers on quartz zero background sample holders and measured on a PW3040/60 sample spinner stage at 1 revolution per second. Diffraction data sets were typically collected in 0.0167° steps for various 2θ ranges and various times. Incident beam optics were chosen with 0.04 rad Soller slits, a 1° divergence slit, a 10 mm mask, and a 2° antiscatter slit. The diffracted beam optics included a 3.4 mm antiscatter slit, 0.04 rad Soller slits, and a nickel filter. Phase identification was carried out using the X'Pert Highscore Plus software suite (version 2.1.0) using the ICDD PDF database.[20]

2.2.2. High-Temperature in Situ Powder X-ray Diffraction. In situ powder X-ray diffraction experiments were carried out using the same PANalytical X'Pert Pro diffractometer as in section 2.2.1 equipped with an Anton Paar HTK2000 high-temperature furnace attachment. The self-masking furnace uses a 10 mm wide Pt-strip heater and is controlled with a Eurotherm 2604 controller. All data were collected with Cu–K$\alpha_{1,2}$ radiation ($\lambda(K\alpha_1)$ = 1.540598 Å, and $\lambda(K\alpha_2)$ = 1.544426 Å) using a diffracted beam Ni filter. Twenty minute diffraction data sets were collected from 2θ = 25° to 2θ = 90° with 0.0167° steps. Samples were mounted directly onto the platinum strip heater and heated from 25 to 1300 °C with diffraction patterns being collected at 25 °C increments in air, flowing O_2, or a dynamic vacuum.

2.3. Powder Neutron Diffraction. Neutron diffraction data were collected on the 800 wire medium-resolution powder neutron diffractometer C2 at the Canadian Neutron Beam Centre (CNBC) at the Chalk River Laboratories in Chalk River, Ontario. Data were collected on indium-doped barium cerate $BaCe_{1-x}In_xO_{3-\delta}$ (x = 0.1, 0.2) at varying temperatures upon heating. Using two detector settings and wavelengths, (i) 2θ = 5–85° with λ = 2.37 Å (d-spacings from 0.7885 to 2.2176 Å) and (ii) 2θ = 35–115° with λ = 1.33 Å (d-spacings from 1.7541 to 27.7203 Å), the d-spacing range from d = 0.7885 Å to d = 27.7203 Å was covered. The samples with masses between 1.3 and 1.6 g were loaded in 9 mm diameter and 60 mm long quartz tubes backfilled with 0.3 bar of oxygen. The sealed quartz tube was placed inside a vanadium can and mounted on a sample rod, which was inserted into a top-loading furnace. This furnace, manufactured by AS Scientific Products Ltd. and modified to suit by CNBC, has a 4 in. diameter cylindrical niobium heating element, allowing for a maximum sample temperature of 1300 °C.

2.4. Rietveld Refinements. Rietveld refinements were carried out with FullProf.2k.[21] The powder X-ray data refinements covering the 2θ range of 30–90° converged with typical χ^2 values between 1.5 and 3.0, whereas higher χ^2 values were obtained for the high-temperature diffractograms where secondary phases were present as known impurities. A total of 20–30 parameters were refined, including unit cell dimensions, sample displacement, peak shape, linearly interpolated background parameters, as well as atomic positions and selected isotropic displacement parameters. Known high-temperature impurity peaks (Ba_2CePtO_6, Pt) were excluded for high-temperature refinements.

2.5. X-ray Photoelectron Spectroscopy. XPS spectra were collected on a Kratos Axis Ultra DLD spectrometer under ultrahigh vacuum (~10^{-9} Torr). Powder samples were mounted on a piece of double-sided Cu tape and attached to the XPS sample holder. Monochromatic Al Kα radiation with a 15 mA emission current and 15 kV anode potential was used for excitation. Elemental scans were acquired with a pass energy of 20 eV. A charge neutralizer was employed to minimize charging. All spectra were calibrated to the C 1s line at 285.0 eV.

3. RESULTS AND DISCUSSION

3.1. Phase Transitions in $BaCe_{0.9}La_{0.1}O_{3-\delta}$. The structural phase transitions of $BaCe_{0.9}La_{0.1}O_{3-\delta}$ were followed using in situ powder X-ray diffraction in oxygen taken at 25 °C increments from 25 to 1300 °C. Figure 2 shows the reduced (pseudo cubic) unit cell parameter evolution during heating from 25 to 1300 °C. The reduced cell parameters (a_{red}) are related to the orthorhombic (a_o, b_o, and c_o) and rhombohedral (a_{rh} and c_{rh}) unit cell parameters according to eqs 2 and 3, respectively

$$\text{Orthorhombic: } a_{red} = a_o/\sqrt{2};\ b_{red} = b_o/2;\ c_{red} = c_o/\sqrt{2} \quad (2)$$

$$\text{Rhombohedral: } a_{red} = a_{rh}/\sqrt{2};\ c_{red} = c_{rh}/2\sqrt{3} \quad (3)$$

All unit cell parameters were obtained from Rietveld refinements using the published crystallographic models for $BaCeO_3$[13] and assuming B-site doping for M^{3+}. Figure 3 illustrates representative Rietveld refinement plots for the orthorhombic, rhombohedral, and cubic phases.

The orthorhombic *Pnma*-to-*Imma* phase transition is only identifiable by the disappearance of a set of very weak

dx.doi.org/10.1021/ic501510u | Inorg. Chem. 2014, 53, 8809–8815

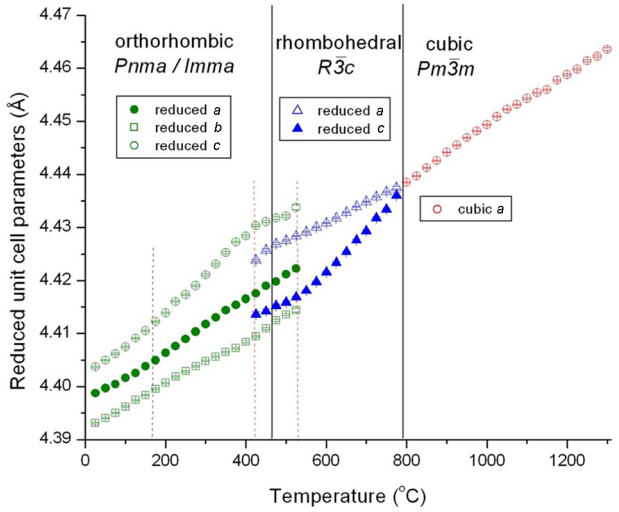

Figure 2. Reduced unit cell parameter (a_{red}) evolution of $BaCe_{0.9}La_{0.1}O_{3-\delta}$ as determined from Rietveld refinements. The solid lines separate structural regimes. The dashed black line indicates the expected *Pnma*-to-*Imma* transition temperature. The red dashed lines indicate the temperature range for the coexistence of the *Imma* and $R\bar{3}c$ phases.

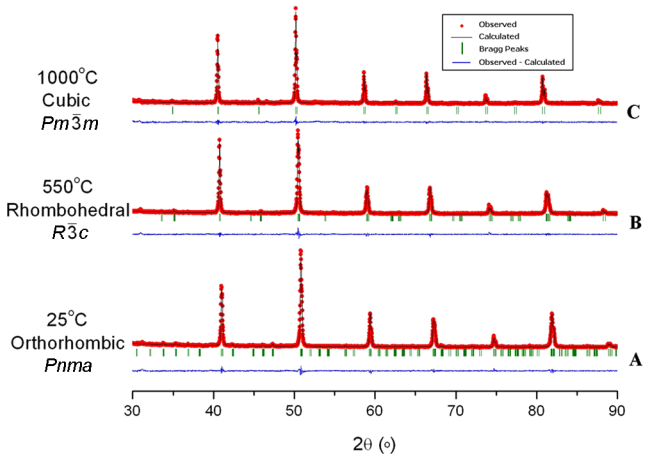

Figure 3. Rietveld refinement plots of $BaCe_{0.9}La_{0.1}O_{3-\delta}$ at (A) 25, (B) 550, and (C) 1000 °C (Note: a negligible trace of double perovskite is present at 1000 °C). The experimental data are indicated as red circles, the best fit as solid black lines, the difference as a solid blue line, and the green tick marks represent expected Bragg positions.

superstructure diffraction peaks that are not readily observable by powder X-ray diffraction. Our in situ powder X-ray diffraction data do not show this transition.

The orthorhombic *Imma*-to-rhombohedral $R\bar{3}c$ (S.G. No. 167) phase transition in $BaCe_{0.9}La_{0.1}O_{3-\delta}$ is observed between 425 and 525 °C in the in situ powder X-ray diffraction data, suggesting a first-order phase transition.

The rhombohedral-to-cubic $Pm\bar{3}m$ (S.G. No. 221) phase transition is observed at 800 °C. Notably, the phase transitions and temperatures for the La-doped barium cerate closely follow the transition temperatures reported by Knight[13] for the parent $BaCeO_3$ phase. Consequently, 10 mol % La^{3+} doping only has a minor impact on the structural details and phase transitions for $BaCeO_3$.

3.2. Transient Ba_2CePtO_6 Double Perovskite Phase. Figure 4 shows a selected angular range ($27.5° \leq 2\theta \leq 30.5°$)

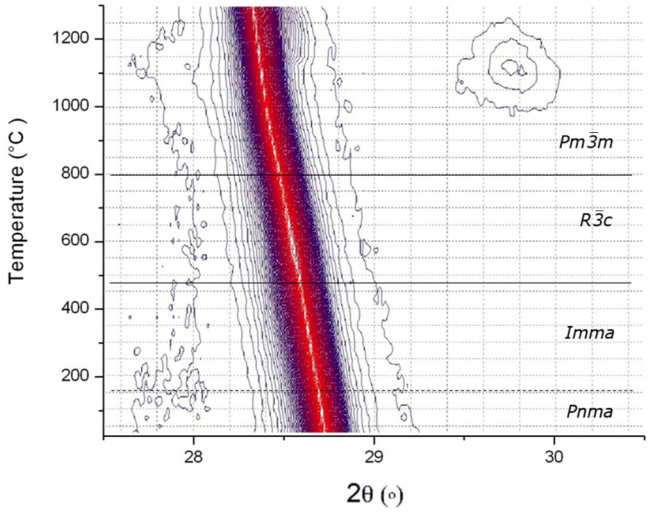

Figure 4. X-ray diffraction contour plot of $BaCe_{0.9}La_{0.1}O_{3-\delta}$ during heating in oxygen flow. The contour lines show linear intensity increase from blue to red. The temperature-dependent phases are indicated in accordance to Figure 2.

of a powder X-ray diffraction contour plot of $BaCe_{0.9}La_{0.1}O_{3-\delta}$ during heating in flowing oxygen from 25 to 1300 °C. During heating, the peak at $2\theta \approx 28.75°$ shifts toward smaller diffraction angles due to overall thermal expansion of the perovskite phase. Between 950 and 1200 °C, a transient peak indicative of a new phase is observed at $2\theta \approx 29.75°$ ($d \approx 3.00$ Å). This transient phase is the double perovskite Ba_2CePtO_6. The double perovskite is formed due to the oxidative platinum uptake from the platinum strip heater in the high-temperature diffractometer furnace. The cubic Ba_2CePtO_6 phase crystallizes in space group $Fm\bar{3}m$ and is a B-site ordered double perovskite with alternating PtO_6 and CeO_6 octahedra. The structure of Ba_2CePtO_6 is illustrated in Figure 5. The double perovskite reported here has a 1:1 ratio of Ce:Pt. This ratio may not be exactly 1:1; however, based on the sizes of the cations and anions in the system, it should be relatively close to unity. Another important note is that there is no compositional change, as the peaks associated with the double perovskite phase do not change positions; the only change is the phase fraction of this phase in the samples.

This double perovskite was first reported by Ouchetto et al.[17] and was found when $BaCeO_3$ was reacted in a Pt crucible in air. Ouchetto et al. proposed the following reaction scheme:

$$2BaCeO_3 + Pt + O_2 \underset{T>1000\ °C}{\overset{T=900-1000\ °C}{\rightleftharpoons}} Ba_2CePtO_6 + CeO_2 \quad (4)$$

Equation 4 describes the oxidative uptake of platinum ($Pt^0 \rightarrow Pt^{4+}$) by $BaCeO_3$; therefore, Ba_2CePtO_6 can only be formed with Pt metal in the presence of oxygen. Consequently, Ba_2CePtO_6 should not be formed when reacting $BaCe_{0.9}La_{0.1}O_{3-\delta}$ on a Pt heater in vacuum. Figure 6 shows the powder X-ray diffractograms collected at 1125 °C on the platinum heater in oxygen flow (red) and in a dynamic vacuum (blue). Because of the absence of oxygen, no double perovskite was formed in vacuum, whereas Ba_2CePtO_6 peaks ($2\theta \approx 29.75°$, 43°, 53°) are clearly visible for the reaction in oxygen. Further support for platinum uptake in an oxidizing atmosphere is obtained from X-ray photoelectron spectroscopy (XPS) measurements. When the doped perovskite is reformed after

dx.doi.org/10.1021/ic501510u | Inorg. Chem. 2014, 53, 8809−8815

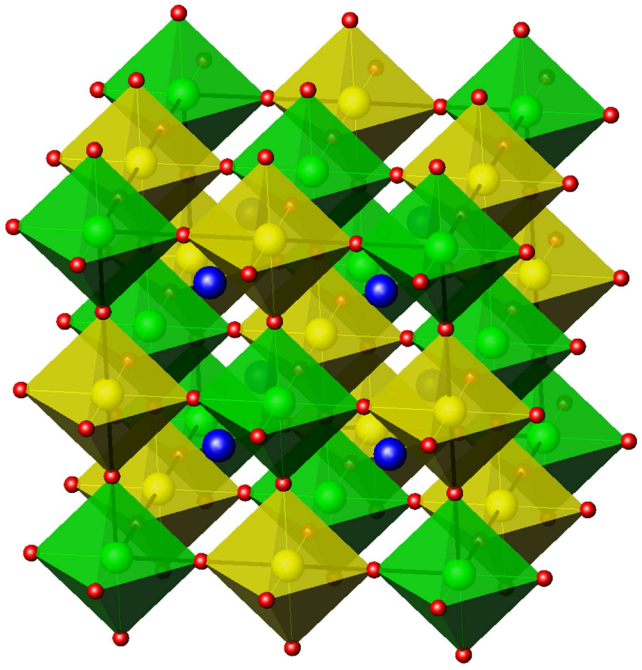

Figure 5. Ba_2CePtO_6 structure where gold octahedra are CeO_6 and green octahedra are PtO_6. Oxide anions are shown as red spheres, and blue spheres represent Ba^{2+} ions.

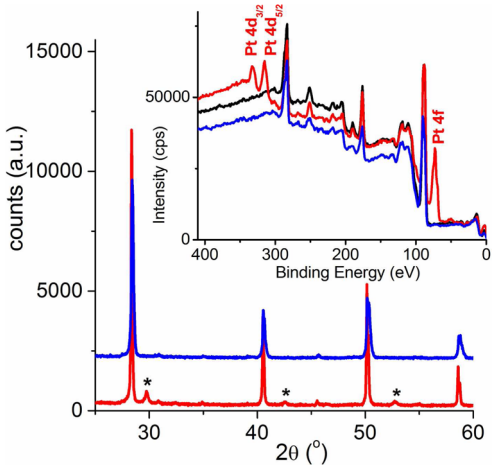

Figure 6. Comparison of powder X-ray diffractograms of $BaCe_{0.9}La_{0.1}O_{3-\delta}$ collected at 1125 °C in a dynamic vacuum (blue) and flowing O_2 (red). Ba_2PtCeO_6 peaks are indicated with ∗. Inset: XPS survey spectra of $BaCe_{0.9}La_{0.1}O_{3-\delta}$ before in situ heating (black), after in situ heating on Pt in flowing O_2 (red), and after in situ heating on Pt in dynamic vacuum (blue). The Pt peaks are labeled in the spectrum.

the double perovskite decomposes, the platinum is released back into the powder and should be seen in the XPS data. The inset in Figure 6 shows the XPS data of $BaCe_{0.9}La_{0.1}O_{3-\delta}$ before in situ heating (black trace) as well as after in situ heating (red trace) in oxygen and vacuum (blue trace) on the platinum heater. The initial sample (before heating) and the sample heated in vacuum show no Pt, whereas the sample heated in oxygen shows strong Pt signals, indicated on the figure. The lack of platinum peaks in any spectrum other than that of the $BaCe_{0.9}La_{0.1}O_{3-\delta}$ after in situ heating in oxygen strongly suggests the transient formation of the double perovskite and confirms the reaction scheme (eq 4) as originally proposed by Ouchetto et al.[17]

3.3. $BaCe_{0.9}In_{0.1}O_{3-\delta}$ Reactivity. $Ce_{1-x}In_xO_{2-\delta}$ cannot be formed directly from CeO_2 and In_2O_3, but it is accessible through $BaCe_{1-x}In_xO_{3-\delta}$ reaction with CO_2.[14] In 2010, Bhella et al. reported the formation pathway of the perovskite and the subsequent carbon dioxide capture reaction using in situ powder X-ray diffraction on a Pt heater.[14] Figure 7 shows a

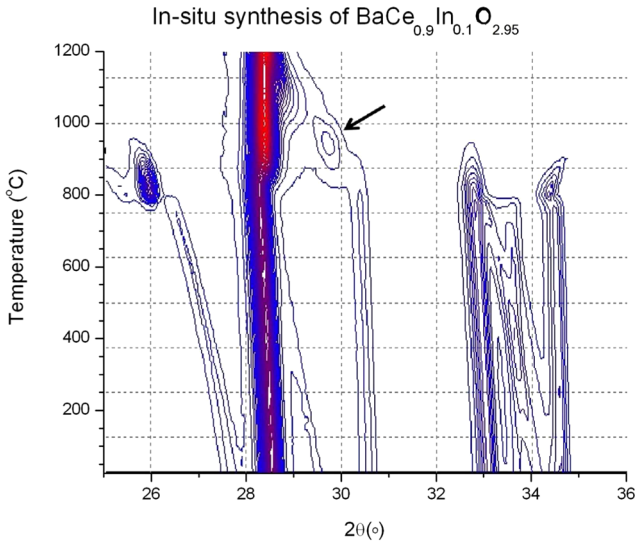

Figure 7. Contour plot of the in situ synthesis of $BaCe_{0.9}In_{0.1}O_{3-\delta}$ (adapted from Bella et al.).[14] The double perovskite Ba_2CePtO_6 phase formation is indicated with an arrow.

powder X-ray diffraction contour plot following the formation of $BaCe_{0.9}In_{0.1}O_{3-\delta}$. All peaks in Figure 7 were assigned to the starting materials ($BaCO_3$(BaO), In_2O_3, and CeO_2) and the final product $BaCe_{0.9}In_{0.1}O_{3-\delta}$. However, one peak (indicated with an arrow) was not assigned. This peak appears at the same diffraction angle and exists over the same temperature range as expected for the Ba_2CePtO_6 double perovskite. This suggests that the double perovskite is not only formed when heating the doped perovskite phase but also during the formation of the perovskite phase from $BaCO_3$, CeO_2, and a B-site dopant.

3.4. High-Temperature Neutron Diffraction Study of $BaCe_{1-x}In_xO_{3-\delta}$. High-temperature neutron powder diffraction experiments were carried out on $BaCe_{0.9}In_{0.1}O_{3-\delta}$ and $BaCe_{0.8}In_{0.2}O_{3-\delta}$ from 25 to 1050 °C. Figure 8 shows the neutron diffractograms from room temperature up to 450 °C. The characteristic (122) and (102) superstructure peaks are consistent with space group *Pnma* (S.G. No. 62) and vanish between 100 and 200 °C as $BaCe_{0.9}In_{0.1}O_{3-\delta}$ forms the *Imma* (S.G. No. 74) structure. The *Pnma*-to-*Imma* transition is observed for $BaCe_{1-x}In_xO_{3-\delta}$ with x = 0.1 and 0.2.

Figure 9 shows the high-temperature powder neutron diffraction data for $BaCe_{0.8}In_{0.2}O_{3-\delta}$ in the presence of Pt (left) and the absence of Pt (right). The disappearance of the (113) peak at approximately 800 °C indicates the rhombohedral-to-cubic phase transition for both samples and is labeled on the figure.

Again, the double perovskite peak is only expected for samples reacted in the presence of platinum. The left diagram of Figure 9 clearly shows the appearance of the (200) double perovskite peak at a *d*-spacing of approximately 4.12 Å for the sample containing Pt. This peak makes its first appearance in

dx.doi.org/10.1021/ic501510u | Inorg. Chem. 2014, 53, 8809−8815

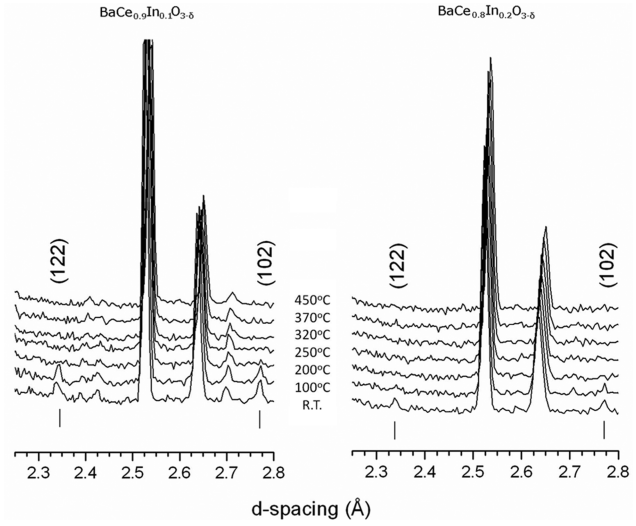

Figure 8. In situ neutron powder diffractograms of $BaCe_{0.9}In_{0.1}O_{3-\delta}$ and $BaCe_{0.8}In_{0.2}O_{3-\delta}$ upon heating from room temperature up to 450 °C for a *d*-spacing range of 2.25−2.8 Å. Note the disappearance of the (122) peak at a *d*-spacing of ≈2.35 Å and the (102) peak at a *d*-spacing of ≈2.78 Å.

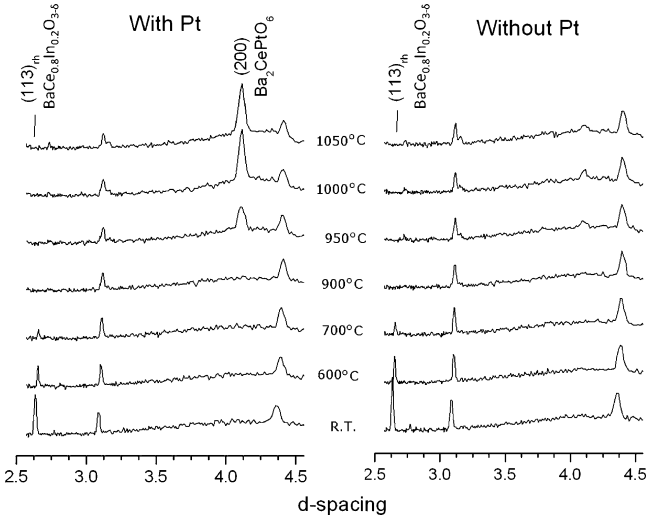

Figure 9. In situ neutron powder diffractograms of $BaCe_{0.8}In_{0.2}O_{3-\delta}$ (a) with Pt and (b) without platinum ground in, from a *d*-spacing of 2.5−4.5 Å. Diffractograms were taken during heating from room temperature to 1050 °C.

the diffractogram at 925 °C, and the peak intensity increases until the last diffractogram was measured at 1050 °C. As expected, this peak is not observed in the in situ neutron diffraction experiment of $BaCe_{0.8}In_{0.2}O_{3-\delta}$ without platinum. A small (temperature-independent) impurity peak is visible at $d \approx$ 4.1 Å between 950 and 1050 °C; this peak is not consistent with the Ba_2CePtO_6 phase.

3.5. In Situ Synthesis of Doped Perovskites. Perovskites with different dopant concentrations ($BaCe_{1-x}In_xO_{3-\delta}$, x = 0.1, 0.2, 0.3, 0.4) were formed in situ, and the powder X-ray diffraction contour plots can be seen in Figure 10. Note that the double perovskite is formed for each of the four compositions. Also important is that, as the molar ratio of indium increases in the doped perovskite, the (110) peak of the $BaCe_{1-x}In_xO_{3-\delta}$ shifts to higher 2θ values. This is due to the smaller ionic radius of indium, $r(In^{3+}(VI))$ = 0.80 Å, compared to that of cerium,

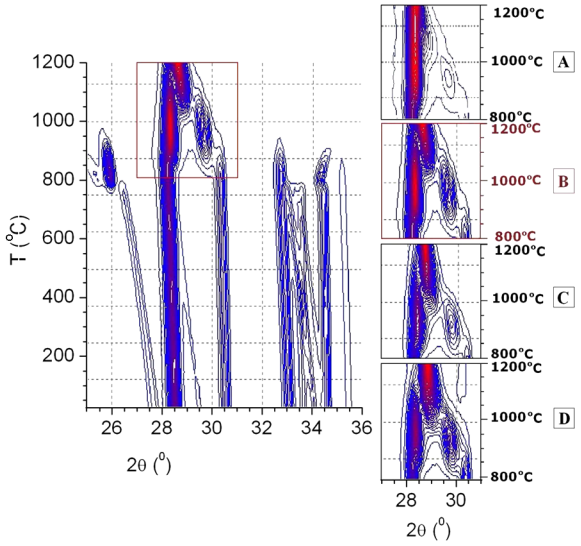

Figure 10. Contour plot of the in situ synthesis of $BaCe_{0.8}In_{0.2}O_{3-\delta}$. The inset shows the area from 2θ = 27° to 31° and temperature ranges from 800 to 1200 °C for (A) $BaCe_{0.9}In_{0.1}O_{3-\delta}$,[14] (B) $BaCe_{0.8}In_{0.2}O_{3-\delta}$, (C) $BaCe_{0.7}In_{0.3}O_{3-\delta}$, and (D) $BaCe_{0.6}In_{0.4}O_{3-\delta}$. The contour lines show linear intensity increase from blue to red.

$r(Ce^{4+}(VI))$ = 0.87 Å.[22] However, the (220) double perovskite peak position (at approximately 29.5−30°) does not change as a function of indium doping. This indicates that the double perovskite does not pick up any significant amount of indium, and we, therefore, conclude from our X-ray in situ studies that the double perovskite forms as nearly pure Ba_2CePtO_6. This raises the question of where the indium resides if it is not incorporated into the double perovskite phase. No In_2O_3 is visible in any of the contour plots shown in Figure 10 at that temperature. The dopant is believed to form a barium-indium oxide phase, possibly $Ba_4In_2O_7$; however, the diffraction peaks for these oxides would largely overlap with the peaks of the perovskite and double perovskite. Consequently, the positive identification of this additional phase is very challenging and may require even higher-resolution powder diffraction data.

Another interesting characteristic of the synthesis contour plots (Figure 10) is that the formation temperatures of the doped perovskites seem to coincide with the decomposition temperature of the double perovskite independent of the dopant concentration. The transient occurrence of the Ba_2CePtO_6 double perovskite could potentially indicate its mechanistic involvement in the formation of $BaCe_{1-x}M_xO_{3-\delta}$ phases by means of oxidative and reductive platinum cycling. In order to support this suggestion, a more in-depth in situ study of the formation of $BaCe_{1-x}M_xO_{3-\delta}$ using a non-platinum heater should follow the formation temperatures of the $BaCe_{1-x}M_xO_{3-\delta}$ phases in the absence of platinum.

3.6. Expansion to Other Trivalent Atoms. Lanthanum and indium were chosen as dopants as they are good candidates that span a wide range of trivalent ion sizes, $r(In^{3+}(VI))$ = 0.80 Å and $r(La^{3+}(VI))$ = 1.03 Å. Since In^{3+} and La^{3+} doped samples showed the same properties, reactivities, and phase diagram evolutions, it is suggested that all lanthanides will follow the same trend. We have confirmed this trend with holmium, yttrium, and lutetium ($r(Ho^{3+}(VI))$ = 0.901 Å; $r(Y^{3+}(VI))$ = 0.90 Å; and $r(Lu^{3+}(VI))$ = 0.86 Å)[22] doped $BaCe_{0.9}M_{0.1}O_{3-\delta}$ samples. As expected, all doped analogues were formed and all

dx.doi.org/10.1021/ic501510u | Inorg. Chem. 2014, 53, 8809−8815

materials consistently formed the Ba_2CePtO_6 transient phase at high temperatures.

3.7. Ex Situ Study of Ba_2CePtO_6. An attempt to make the Ba_2CePtO_6 ex situ was made by grinding together stoichiometric amounts of $BaCeO_3$ and Pt sponge. Pt sponge was required for this synthesis as it seems to be a surface reaction, which does not easily form in the bulk of the powder. Different Pt-containing starting materials were attempted, and Pt sponge seems to work best. A pellet was formed and heated under a flow of oxygen for 80 h at 950 °C before rapidly quenching the sample to room temperature. The resulting pellet was reground and reheated for 264 more hours (11 days) in flowing oxygen and then again quenched to room temperature. Figure 11

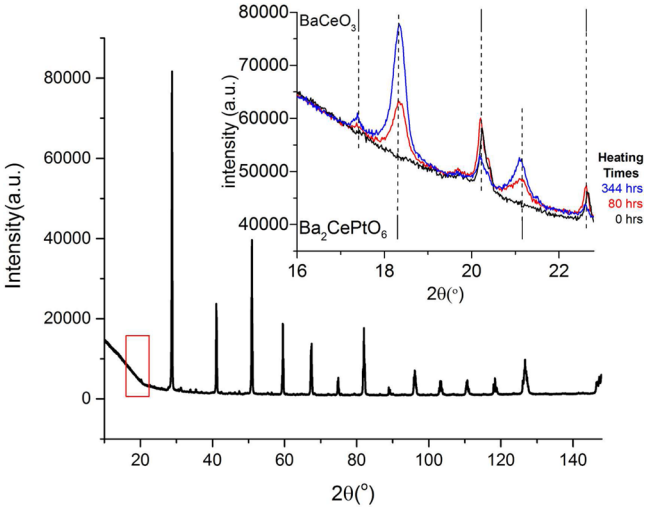

Figure 11. X-ray diffractogram from $2\theta = 10°$ to 148° of the $BaCeO_3$ starting material. The inset is an additional experiment that focuses on small superstructure peaks between $2\theta = 16.0°$ and 22.8°. The black line represents $BaCeO_3$ before heating, the red line represents product after heating $BaCeO_3$ and Pt metal for 80 h in flowing oxygen, and the blue line represents product after heating for an additional 264 h under flowing oxygen. The tick marks indicate the Bragg peak positions for Ba_2CePtO_6 and $BaCeO_3$.

shows the $BaCeO_3$ starting material before it was reacted with platinum (black line). The inset is a comparison of the diffractograms of $BaCeO_3$ before heating, the sample after heating for 80 h (first heating, red line), and the sample after heating for an additional 264 h (blue line). This inset is not a zoom of the diffractogram; it is an additional experiment that focuses on small superstructure peaks (the (111) and (200) Ba_2CePtO_6 peaks are both less than 4% of the main peak) that are found only if the Ba_2CePtO_6 double perovskite is present. A few very weak impurity peaks are found in the diffractograms; however, these impurity peaks are only seen as a result of the extremely long counting times required to obtain good intensities for the superstructure peaks and would normally be buried in the noise.

Equation 4 suggests that, if Ba_2CePtO_6 is formed, CeO_2 will also be formed and the corresponding peaks should be visible in the diffractograms. The CeO_2 main peak (111) is hidden underneath the main peak of $BaCeO_3$; however, the (200) peak is present at 33.1° where there is no peak for either $BaCeO_3$ or Ba_2CePtO_6. The intensities of all CeO_2 and Ba_2CePtO_6 peaks grow upon longer heating times, while a decrease in all peaks associated with $BaCeO_3$ was observed. This can more easily be seen by calculating integrated intensities of the (111) Ba_2CePtO_6 peak found at $2\theta \approx 18.1°$ and of the combined (101) and (020) peaks of $BaCeO_3$ found at $2\theta \approx 20.0°$. The intensity of the (111) Ba_2CePtO_6 peak increased from 3844(309) cts after heating for 80 h to 8350(300) cts upon further heating. The $BaCeO_3$ peak ((101) and (020)) decreased from 2522(189) cts after the first heating to 989(181) cts after the second heating. Calculating a ratio of these values clearly shows the conversion from the perovskite to the double perovskite. After the first heating, the $Ba_2CePtO_6(111)/BaCeO_3(101,002)$ intensity ratio is 1.5(2) and increases to 8.4(1.8) after the second heating. This strongly supports the formation of Ba_2CePtO_6.

4. CONCLUSIONS

Phase-pure indium- and lanthanum-doped $BaCeO_3$ were synthesized, and the phase evolutions of $BaCe_{0.9}La_{0.1}O_{3-\delta}$ and $BaCe_{1-x}In_xO_{3-\delta}$ ($x = 0.1, 0.2$) were followed by in situ powder X-ray and in situ neutron diffraction. The doped phases follow the same phase transition sequence as that previously reported for the parent $BaCeO_3$ phase. However, when heated in the presence of platinum, the doped perovskite material reacts with platinum and forms the Ba_2CePtO_6 double perovskite. This phase was characterized using XPS as well as powder diffraction (both neutron and X-ray) in different atmospheres. On the basis of the X-ray diffraction studies, this double perovskite is devoid of any dopant regardless of the identity of the dopant or the amount of dopant in the sample. The Ba_2CePtO_6 double perovskite is also formed during the in situ synthesis of doped $BaCeO_3$ on a Pt heater, and it is further found that the doped perovskite forms as the double perovskite decomposes. It is unknown what affect the double perovskite phase has on the formation of the doped perovskite, but it is suggested that the formation could be catalyzed or aided by the platinum-containing double perovskite.

AUTHOR INFORMATION

Corresponding Author

*E-mail: Mario_Bieringer@umanitoba.ca. Phone: (204) 474-6258. Fax: (204) 474-7608 (M.B.).

Notes

The authors declare no competing financial interest.

ACKNOWLEDGMENTS

The authors are grateful to Dr. Kevin McEleney (University of Manitoba) for the XPS measurements and Dr. V. Thangadurai for providing additional samples. M.B. acknowledges the support from NSERC, CFI, and MIF. We thank the Canadian Neutron Beam Center (CNBC) in Chalk River, Ontario, for providing access to the DUALSPEC neutron diffractometer and for technical support from Raymond Sammon and Chad Boyer.

REFERENCES

(1) Bhalla, A. S.; Guo, R.; Roy, R. *Mater. Res. Innovations* **2000**, *4*, 3–26.
(2) Iwahara, H. *Solid State Ionics* **1996**, *86–88*, 9–15.
(3) Roder-Roith, U.; Rettig, F.; Sahnerm, K.; Roder, T.; Janek, J.; Moos, R. *Solid State Ionics* **2011**, *192*, 101–104.
(4) Kreuer, K.-D. *Chem. Mater.* **1996**, *8*, 610–641.
(5) Kreuer, K.-D.; Paddison, S. J.; Spohr, E.; Schuster, M. *Chem. Rev.* **2004**, *104*, 4637–4678.
(6) de Souza, E. C. C.; Muccillo, R. *Mater. Res.* **2010**, *13*, 385–394.

(7) Glöckner, R.; Islam, M. S.; Norby, T. *Solid State Ionics* **1999**, *122*, 145−156.
(8) Katahira, K.; Kohchi, Y.; Shimura, T.; Iwahara, H. *Solid State Ionics* **2000**, *138*, 91−98.
(9) Virkar, A. N.; Maiti, H. S. *J. Power Sources* **1985**, *14*, 295−303.
(10) Knight, K. S.; Bonanos, N. *J. Mater. Chem.* **1994**, *4*, 899−901.
(11) Knight, K. S. *Solid State Ionics* **2000**, *127*, 43−48.
(12) Knight, K. S. *Solid State Ionics* **1994**, *74*, 109−117.
(13) Knight, K. S. *Solid State Ionics* **2001**, *145*, 275−294.
(14) Bhella, S. S.; Shafi, S. P.; Trobec, F.; Bieringer, M.; Thangadurai, V. *Inorg. Chem.* **2010**, *49*, 1699−1704.
(15) Scherban, T.; Villeneuve, R.; Abello, L.; Lucazeau, G. *J. Raman Spectrosc.* **1993**, *24*, 805−814.
(16) Scherban, T.; Villeneuve, R.; Abello, L.; Lucazeau, G. *Solid State Commun.* **1992**, *84*, 341−344.
(17) Ouchetto, K.; Archaimbault, F.; Pineau, A.; Choisnet, J. *J. Mater. Sci. Lett.* **1991**, *10*, 1277−1279.
(18) Ouchetto, K.; Archaimbault, F.; Choisnet, J.; Et-Tabirou, M. *Mater. Chem. Phys.* **1997**, *51*, 117−124.
(19) Casapu, M.; Grunwaldt, J.-D.; Maciejewski, M.; Baiker, A.; Eckhoff, S.; Wittrock, M. *J. Catal.* **2007**, *251*, 28−38.
(20) *PDF-2 Database*; International Centre for Diffraction Data: Newtown Square, PA, 2003.
(21) Rodriguez-Carvajal, J. *Full Prof.2k*, Vers. 4.40; 2008. http://www.ill.eu/sites/fullprof/.
(22) Shannon, R. D. *Acta Crystallogr.* **1976**, *A32*, 751−767.